Available online at www.sciencedirect.com
ScienceDirect
Trans. Nonferrous Met. Soc. China 33(2023) 1803−1813
Transactions of Nonferrous Metals Society of China
www.tnmsc.cn

Effects of Cu additions on microstructure and mechanical properties of as-cast CrFeCoNiCu$_x$ high-entropy alloy

Qiang HU[1], Hai-ling WANG[2], Li-hua QIAN[2], Liang-cai ZENG[3,4], Qiang WANG[3,4], Xin-wang LIU[5]

1. Institute of Applied Physics, Jiangxi Academy of Sciences, Nanchang 330029, China;
2. School of Physics, Huazhong University of Science and Technology, Wuhan 430074, China;
3. Key Laboratory of Metallurgical Equipment and Control Technology, Ministry of Education, School of Machinery and Automation, Wuhan University of Science and Technology, Wuhan 430081, China;
4. Hubei Key Laboratory of Mechanical Transmission and Manufacturing Engineering, School of Machinery and Automation, Wuhan University of Science and Technology, Wuhan 430081, China;
5. State Key Laboratory of Materials Processing and Die & Mould Technology, School of Materials Science and Engineering, Huazhong University of Science and Technology, Wuhan 430074, China

Received 28 December 2021; accepted 30 March 2022

Abstract: The influences of Cu additions on the microstructural evolution and room-temperature tensile properties of the as-cast CrFeCoNi were investigated in detail. The results revealed that the structure of the alloy changed from a FCC single-phase to FCC1 plus FCC2 dual-phase by adding Cu element. The FCC2 phase was determined to be Cu-rich phase existing in the inter-dendrite region, and its volume fraction increased with the increase of Cu additions. The formation of Cu-rich inter-dendrite was mainly ascribed to the liquid-phase separation induced by the large positive mixing enthalpy between Cu and other metallic elements. The yield and ultimate tensile strengths against the Cu content displayed a positive correlation due to the enhancement of short-range obstacles to dislocations slip, while the more significant superposition of stress field produced by the dislocation piling-ups at grain boundaries of Cu-containing high-entropy alloys led to a small fracture strain.

Key words: high-entropy alloy; Cu-rich phase; microstructure; tensile strength; fracture strain

1 Introduction

For centuries, incorporating small amounts of a few secondary elements into a principal element has been the basic strategy for material design. Although new type of alloys based on various principal elements, such as TiAl and NiAl, have been developed in recent years, the total number of the principal elements is considerably limited. In 2004, YEH et al [1] and CANTOR et al [2] first put forward high-entropy alloys (HEAs) that are based on mixing five or more principal elements in concentrations of 5−35 at.% (usually nearly equiatomic), which has broken through the traditional alloy design strategy. Due to the combination of high strength and ductility [3,4], excellent corrosion resistance [5,6], high temperature microstructural and mechanical stability [7,8], etc., HEAs have attracted much attention since they were proposed. Among the various HEA systems, the equiatomic CrFeCoNi alloy with face-centered-cubic (FCC) structure is not only one of the earliest reported HEA but also one of the extensively studied HEA [9−12]. The single FCC structured HEA usually exhibits

Corresponding author: Hai-ling WANG, Tel: +86-13469963897, E-mail: hlwang2016@hust.edu.cn;
Qiang WANG, Tel: +86-15527617385, E-mail: wangqiang2018@wust.edu.cn
DOI: 10.1016/S1003-6326(23)66223-5

excellent ductility and fracture toughness [13], but relatively low strength [14]. Similar to the conventional alloys, the mechanical performances of the HEAs are mainly determined by their compositions and microstructures, and the strengthening strategies of conventional alloys, such as solid-solution hardening, precipitation hardening, are also suitable for the HEAs.

It has been proved that the precipitation strengthening is an effective method to improve the strength of the FCC structured HEA [15−17]. Recent research on the microstructures of HEAs has suggested that copper is a commonly used precipitation-hardening element because of its low solubility in HEA [18−20]. In general, the FCC single-phase structured HEAs containing Cu can significantly improve their mechanical properties, which is mainly ascribed to the precipitation-strengthening effect of the Cu-rich phase precipitated from the FCC-solution matrix [16,21,22]. PENG et al [16] reported that during the process of deformation the uniformly distributed Cu-rich phase precipitated in the FCC-solution matrix acted as the obstacles to dislocation sliding, thus leading to a drastic improvement of the strength. The aforementioned studies have clarified that Cu additions had the precipitate-strengthening effect on the HEA, but there is a lack of a comprehensive and systemic in-depth study upon evolution of the Cu-rich precipitates with Cu content, as well as the corresponding relationship between the Cu-rich precipitates and the mechanical properties.

Therefore, in the present work, the equiatomic CrFeCoNi system, one of the widely investigated FCC single-phase structured HEA, was selected as the base alloy. For the purpose of understanding the evolution law of the Cu-rich precipitates and acquiring the optimal comprehensive properties (involving strength and ductility), a series of HEAs containing Cu were prepared, i.e., $CrFeCoNiCu_x$ (x=0, 0.3, 0.5, 0.7). The microstructure features, phase constituents, precipitation behaviors of Cu-rich phase and room-temperature tensile properties of the Cu-containing HEAs were studied. Moreover, the influence of Cu-rich precipitation phases on the relevant deformation mechanism was discussed.

2 Experimental

The Cu-containing HEAs $CrFeCoNiCu_x$ (x=0, 0.3, 0.5, 0.7) were melted by vacuum arc furnace, and the details could refer to Ref. [23]. For the sake of simplicity, the Cu-containing HEAs were denoted as Cu_0, $Cu_{0.3}$, $Cu_{0.5}$ and $Cu_{0.7}$, respectively. Raw materials for preparation of the above HEAs were metal particles or blocks, and their purity was greater than 99.95 wt.%. After arc-melting, the button ingots were drop-cast into a rectangular copper mold with dimensions of 10 mm × 17 mm × 80 mm. In order to characterize the as-cast HEAs, the samples for microstructure observations were firstly cut by a wire cut electrical discharge machine from the ingots, and then manually ground by using abrasive papers, followed by electro-chemically polished in a mixed solution of 20% $HClO_4$ and 80% C_2H_5OH (in vol.%) at 25 V and room temperature for 30 s. Phase identification was carried out on a Shimadzu XRD−7000S X-ray diffractometer (XRD) with Cu K_α radiation (λ=0.15418 nm). Recording of the XRD patterns was performed in the 2θ range of 20°−100°, and the scanning rate was 5 (°)/min. An FEI Quanta 200 field emission scanning electron microscope (FE-SEM) equipped with an energy dispersive spectroscope (EDS) was used to characterize the microstructure and chemical compositions. During microstructure investigations, the working parameters of SEM were set as follows: acceleration voltage of 15 kV, working distances of 9.4−10.1 mm, magnification times of 500−2000, and Iprobe current of 10 pA. Further investigations on the fine scale microstructure were carried out by G2 F30 transmission electron microscope (TEM). The foils for TEM observations extracted from the HEA samples were manually ground down to about 90 μm, and then punched into discs with a diameter of 3 mm, and finally twin-jet polished in a solution of 90 vol.% glacial acetic acid and 10 vol.% $HClO_4$ at room temperature.

The mechanical properties of the Cu-containing HEAs were characterized through the room-temperature tensile tests. The tensile specimens with gauge dimensions of 10 mm (length) × 2.5 mm (width) × 1.2 mm (thickness) were machined by electric discharge machine and the tensile test was carried out using a SHIMADZU AG−100KN materials testing machine. The strain rate was 5.0×10^{-4} s^{-1}. After tensile tests, the fracture appearance, crack propagation and deformed behavior of the HEAs were analyzed by SEM and TEM.

3 Results and discussion

3.1 Phase constituent

Figure 1(a) shows the XRD patterns of the as-cast CrFeCoNiCu$_x$ HEAs. As can been, the Cu$_0$ HEA displays a single-phase, and the lattice constant is calculated to be 0.3567 nm, which is similar to the result reported by WANG et al [10]. In contrast, as a certain amount of Cu is incorporated into the CrFeCoNi, i.e., Cu$_{0.3}$ and Cu$_{0.5}$, there is a diffraction peak appearing at the 2θ angle of around 75.2°, indicating the formation of another phase. Referring to the standard database, it is suggested that the diffraction peak at 2θ=75.2° also corresponds to the phase with FCC structure, denoted as FCC2 hereafter. With a further increase in the Cu content, the Cu$_{0.7}$ is also composed of FCC1 plus FCC2. Therefore, it can be concluded that the phase constituent of the HEA changes from FCC single-phase structure to FCC1 plus FCC2 dual-phase structure by the addition of Cu. It should be noted that there are more diffraction peaks of FCC2 phase appearing in the diffraction pattern of Cu$_{0.7}$, i.e., the diffraction angle at 2θ of about 50.8°, which reveals that the volume fraction of FCC2 phase rises with the increase of Cu additions. Moreover, the lattice constants of the FCC1 and FCC2 phases against the Cu content are calculated from their XRD patterns and the corresponding results are plotted in Fig. 1(b). It can be seen that the lattice constant of FCC1 solid solution displays a slight drop with the increase of Cu content, while the lattice constant of FCC2 presents an opposite trend, increasing from 0.3610 nm to 0.3648 nm. The lattice constants of FCC1 and FCC2 phases show opposite trends, mainly due to the difference of atomic radius. The atomic radii of Cr, Fe, Co, Ni and Cu are 0.125, 0.124, 0.125, 0.125 and 0.128 nm, respectively. With the increase of Cu content, more Cu atoms are involved in the Cu-rich phase, thus leading to the expansion of the lattice. Meanwhile, the Cr, Fe, Co and Ni atoms repelled by the Cu-rich phase are dissolved in the FCC1 and occupy the sites of the Cu atoms in the lattice, which causes the lattice to shrink.

3.2 Microstructure

Figure 2 shows the back-scattered electron (BSE)-SEM images of CrFeCoNiCu$_x$ alloys. It can be seen that the microstructure of Cu$_0$ alloy is composed of coarse grains. In addition, the EDS surface scanning analysis is performed on three adjacent grains, and the corresponding results are displayed in Fig. 3. It is found that the elements are uniformly distributed and no element enrichment or depletion occurs in different grains or even at grain boundary. As shown in Table 1, the actual chemical composition revealed by EDS analysis at the points indicated by the blue cross symbols is almost identical with the normal composition of Cu$_0$ alloy.

With the increase of Cu additions, the BSE-SEM images show that the microstructures of Cu$_{0.3}$, Cu$_{0.5}$ and Cu$_{0.7}$ alloys exhibit the typical feature of dendrite crystal structure, in which dendrite is grey contrast and inter-dendrite is dark contrast. The chemical compositions of the dendrite and inter-dendrite regions are characterized by the EDS surface scanning, and the results are shown in Figs. 4(a−g). It is evident that compared with the dendrite, the inter-dendrite region is characterized by rich Cu and poor Cr, Fe, Co and Ni, which suggests that the Cu element tends to segregate within the inter-dendrite regions. Considering the

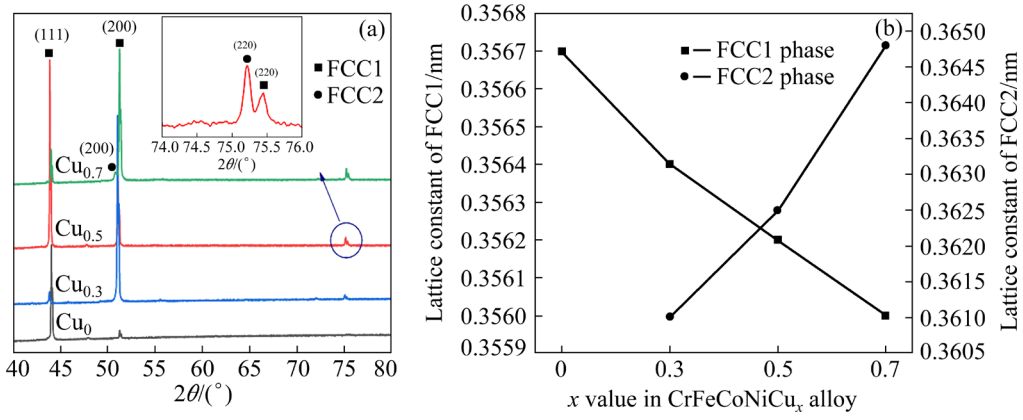

Fig. 1 XRD patterns of as-cast HEAs (a) and lattice constants of FCC1 and FCC2 (b)

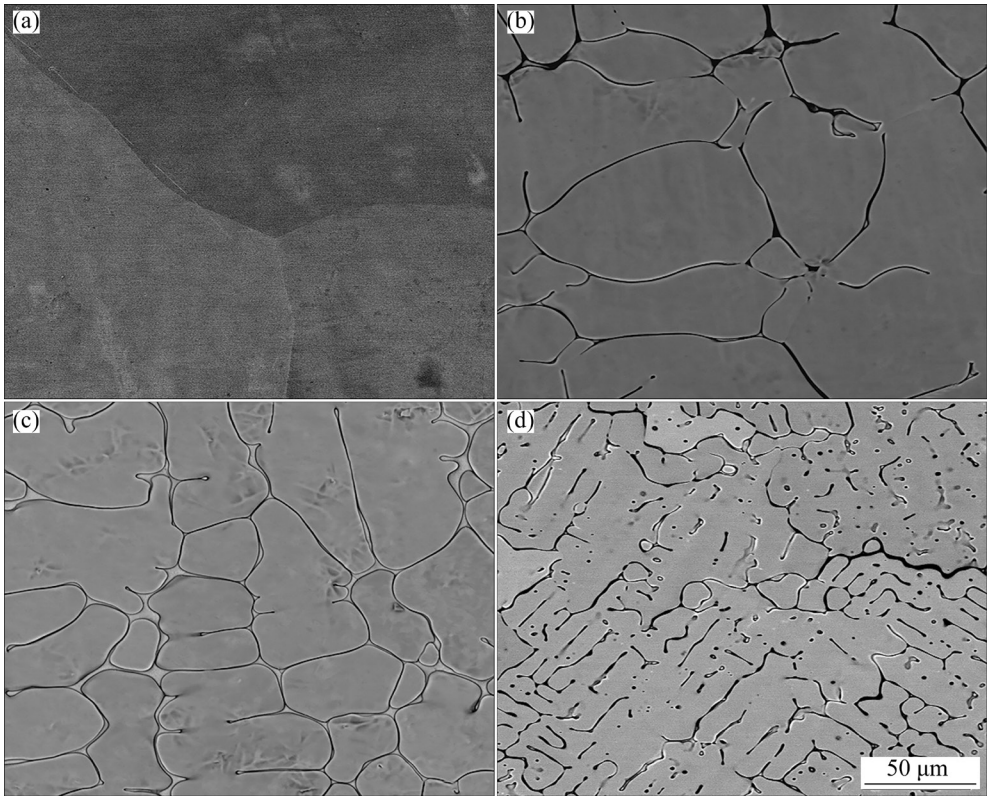

Fig. 2 BSE-SEM images of CrFeCoNiCu$_x$ alloys: (a) Cu$_0$; (b) Cu$_{0.3}$; (c) Cu$_{0.5}$; (d) Cu$_{0.7}$

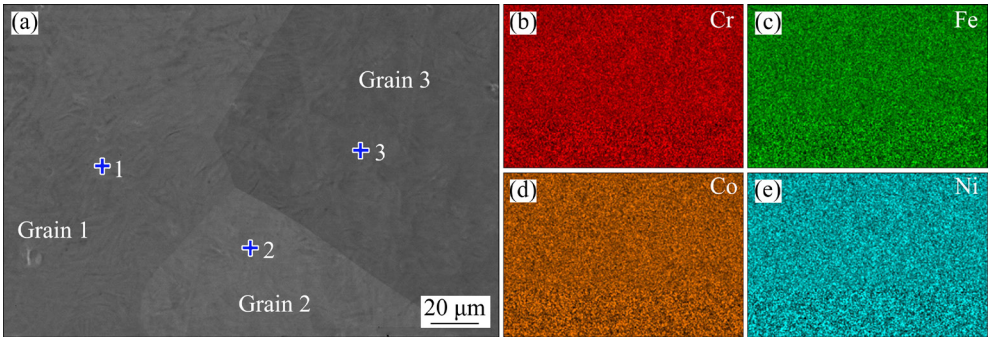

Fig. 3 EDS surface scanning analysis results of adjacent three grains

Table 1 EDS point analysis results of Fig. 3(a) on Cu$_0$ alloy (at.%)

Point No.	Cr	Fe	Co	Ni
1	25.82	24.84	24.92	24.42
2	25.17	25.03	24.44	25.36
3	25.33	24.75	25.03	24.89

fact that the FCC2 phase contains a considerable content of Cu (much higher than its nominal composition) and the lattice constant of pure Cu (~0.361 nm) is close to that of FCC2 phase (ranging from 0.3610 to 0.3648 nm), and based on the results of XRD and SEM, it can be deduced that the formation of the FCC2 phase is due to the Cu segregation, and its crystal structure is similar to that of the copper.

Additionally, Fig. 4(g) shows a representative SEM image of Cu$_{0.7}$ alloy at higher magnification, and it indicates that there are some particles existing within the dendrite. The EDS line scanning across the precipitated particle and the matrix reveals that the former contains much higher contents of Cu than the latter, as shown in Fig. 4(h). The granular phase existing within the dendrite is also essentially Cu-rich inter-dendrite phase. This is due to the fact that during the solidification, as the dendrites continue to grow, the adjacent dendrites

connect to each other, which makes the area between the dendrites become smaller. As a result, only granular inter-dendritic regions are left.

In order to further identify the phase constituent of the Cu-containing HEA, the bright-field TEM image and selected area electron diffraction (SAED) patterns of $Cu_{0.5}$ alloy are exhibited in Fig. 5. The SAED results reveal that both the Cu-rich and Cu-depleted phases have the same crystal structure (FCC structure). This is consistent with the data detected by XRD. Hence, combined with XRD, SEM and TEM observations, the Cu-depleted and Cu-rich phases are deduced to be FCC1 and FCC2, respectively. According to the contrast difference in SEM images, the volume fraction of FCC1 phase and FCC2 phase can be quantitatively measured by using Image Pro plus software. In order to ensure the accuracy of the measurement data, we have investigated the microstructure of different parts of the ingot, and at

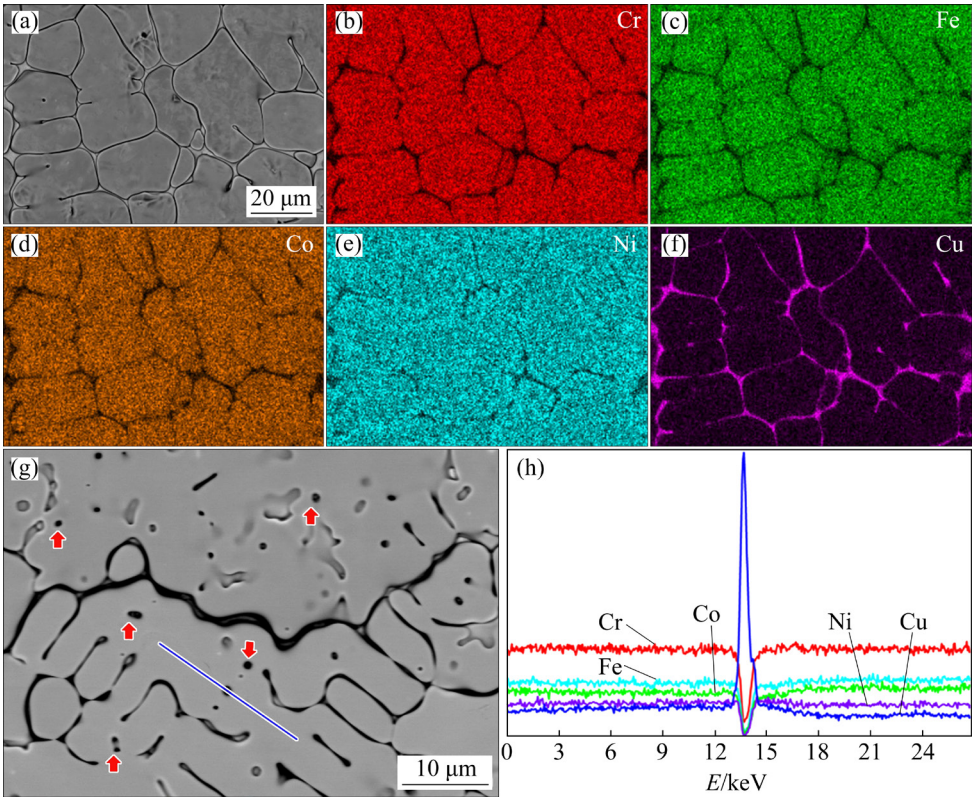

Fig. 4 EDS surface scanning results of $Cu_{0.5}$ alloy (a−f), representative magnified SEM image of $Cu_{0.7}$ alloy (g) and EDS line scanning results across particle phase and matrix in $Cu_{0.7}$ alloy (h)

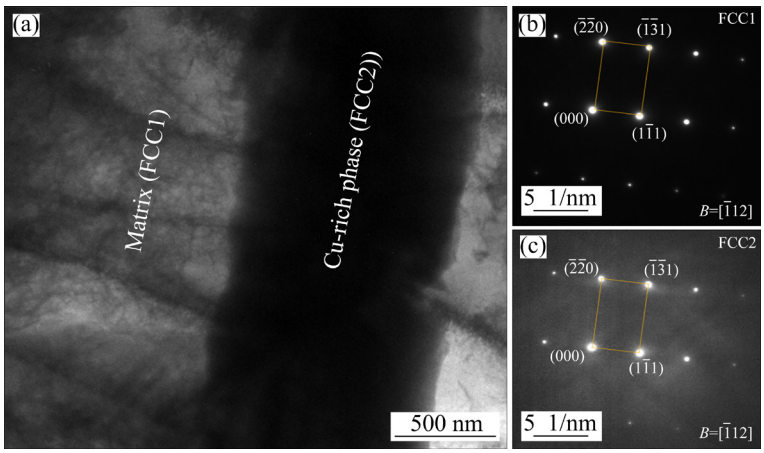

Fig. 5 Bright-field TEM image of $Cu_{0.5}$ alloy (a), and selected area electron diffraction (SAED) patterns of Cu-depleted (b) and Cu-rich (c) phases

least 15 SEM images are measured for each part. As shown in Fig. 6, the volume fraction of FCC2 phase is measured to be 2.6%, 3.4% and 7.6% when the x value in $CrFeCoNiCu_x$ alloy reaches 0.3, 0.5 and 0.7, respectively.

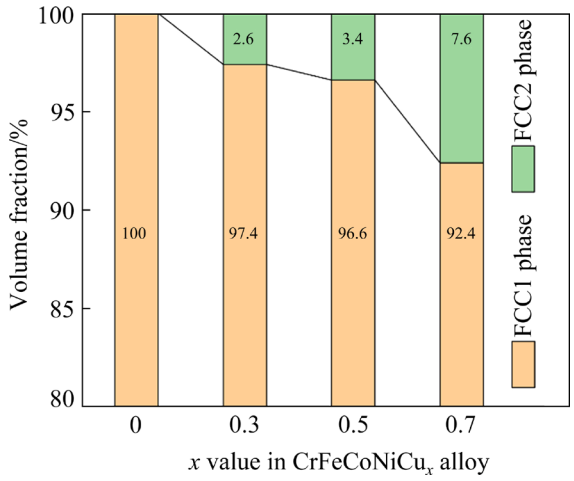

Fig. 6 Volume fraction of FCC1 and FCC2 phases versus x value in $CrFeCoNiCu_x$ alloy

The formation of Cu-rich inter-dendrite region is mainly due to the occurrence of liquid-phase separation prior to solidification, in which the initial liquid-phase has been separated into Cu-rich and Cu-depleted regions. It means that there is a small quantity of liquid phase nucleation, leading to the formation of droplets before the phase transformation of liquid to solid. This phenomenon of liquid separation has already been reported in Cu-bearing alloy systems [18,20]. Previous studies have revealed that the mixing enthalpy of the alloy is responsible for the liquid phase separation. As the mixing enthalpies of Cu and other four elements (Cr, Fe, Co, Ni) are large positive ($\Delta H_{\text{mix}}^{\text{Cu-Cr}}$=12 kJ/mol, $\Delta H_{\text{mix}}^{\text{Cu-Co}}$=6 kJ/mol, $\Delta H_{\text{mix}}^{\text{Cu-Ni}}$=4 kJ/mol, $\Delta H_{\text{mix}}^{\text{Cu-Fe}}$=13 kJ/mol), the Cu element is rejected by Cr, Fe, Co and Ni. Therefore, in the present work, the relatively high positive mixing enthalpy between Cu and other elements makes Cu atoms segregate towards the inter-dendrite during solidification process, eventually leading to the generation of Cu-rich inter-dendrite phase. Meanwhile, it is worth noting that the enrichment of Cu in the Cu-containing HEAs is responsible for the smaller grain size. The formed Cu-rich regions before solidification can act as the heterogeneous nucleation sites, thus leading to a sharp increase in the number of grains. Moreover, the generation of the Cu-rich phase in the inter-dendrite region can further inhibit the grain growth.

Moreover, detailed investigation suggests that there are a few nanoscale globular particles distributed within the Cu-rich phase, as indicated by arrows in Fig. 7(a). Based on the results of SAED (Fig. 7(b)) and TEM−EDS (Fig. 7(c)), the globular particles are identified to be Cu-rich phase with face-centered cubic structure. The formation of Cu-rich particles in FCC2 phase is mainly related to the occurrence of the quasi-peritectic reaction [20]. The solidification process of the Cu-containing HEA includes two stages. At first, the Cu-depleted dendrite solid solution phase nucleates from the liquid at the initial stage of solidification, and then the peritectic reaction of Cu-depleted dendrite phase and liquid phase occurs, leading to the formation of Cu-rich inter-dendrite phase. As Cu element in the Cu-rich inter-dendrite phase is supersaturated, the superfluous Cu atoms will accumulate within the Cu-rich inter-dendrite region during the subsequent cooling process, which finally leads to the generation of Cu-rich globular particles.

3.3 Mechanical properties

Figure 8(a) shows the typical tensile stress−strain curves of the $CrFeCoNiCu_x$ alloys at room temperature, and the yield strength, ultimate strength and fracture elongation as a function of Cu additions are plotted in Fig. 8(b). It reveals that the Cu-free HEA presents a yield strength of 145 MPa and an ultimate tensile strength of 420 MPa. These results are similar to those reported by other researchers [14]. An increase in the Cu additions leads to an improvement of yield strength, and the $Cu_{0.7}$ alloy possesses the highest yield strength of 530 MPa, which is 385 MPa higher than that of the Cu_0 alloy. In contrast, the ultimate tensile strength increases first and then decreases with the increase of Cu additions. Specifically, compared with the Cu_0 alloy, the ultimate tensile strength of $Cu_{0.3}$ and $Cu_{0.5}$ is improved 750 and 805 MPa, respectively, while the ultimate tensile strength of the $Cu_{0.7}$ alloy is 65 MPa lower than that of the $Cu_{0.5}$ alloy. Additionally, it should be noted that the addition of Cu results in a significant decrease in fracture elongation.

In the present work, the improvement of the yield strength assisted by the addition of Cu is

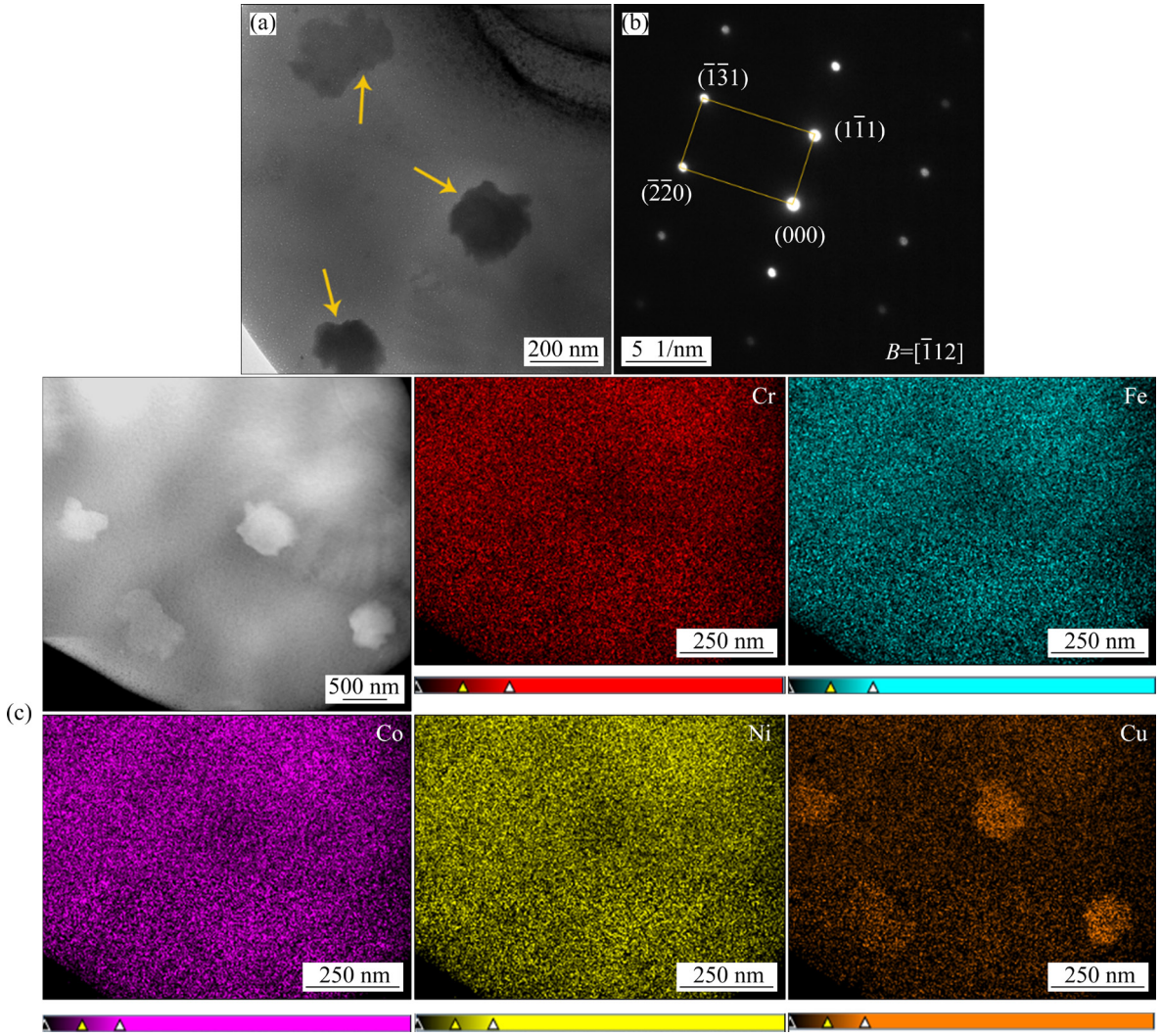

Fig. 7 Bright field TEM image (a), SAED (b) and TEM−EDS results (c) of globular particles within FCC2 phase

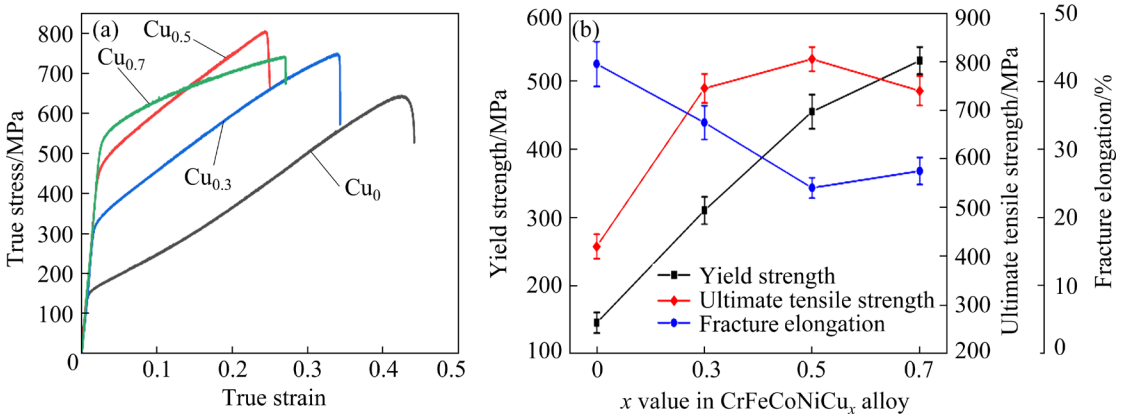

Fig. 8 Tensile true stress−strain curves of $CrFeCoNiCu_x$ alloys (a) and variations of yield strength, ultimate tensile strength and fracture elongation versus Cu additions (b)

mainly due to the greater resistance of dislocation movement. The yield strength (σ_y) of polycrystalline materials can be expressed as

$$\sigma_y = \bar{m}\tau_{CRSS} \quad (1)$$

where m means the reciprocal of Schmidt factor, determined by the orientation of the slip system with respect to the tensile axial, and $\bar{m}$ is a suitable average for the polycrystalline. τ_{CRSS} is

critical resolved shear stress when plastic initiates, which strongly depends on the structural characteristics of materials, as well as test conditions. Under the test conditions of this work, the critical resolved shearing stress can be represented by

$$\tau_{CRSS} = \tau_a + \tau^* \quad (2)$$

where τ_a is the athermal (i.e., temperature-independent) component of the stress, and τ^* represents the thermally dependent temperature component of the stress. It is worth noting that the two components of τ_{CRSS} are related to the microstructural features. The athermal component arises from the stress required to move dislocations in the presence of long-range internal stress fields, i.e., stress field present over distances is larger than atomic dimensions. On the other hand, τ^* represents the resistance to dislocation motion presented by short-range obstacles, existing over distance sufficiently small so that thermal energy is useful for surmounting them. In the present work, the addition of Cu causes lattice distortion and the degree of distortion becomes intensified with the increase of Cu content, which can be verified by the results of lattice calculation (as shown in Fig. 1(b)). The stress field generated by the lattice distortion will interact with the stress field of dislocations. This will result in the enhancement of τ^*, thus contributing to a larger τ_{CRSS}. Apart from that, grain boundaries also have a significant effect on τ^*. As shown in Fig. 2, the formation of Cu-rich phase in the Cu-containing alloys significantly refines the grain size, which correspondingly increases the proportion of grain boundaries. Both small-angle grain boundary and high-angle grain boundary can be regarded as the assembly of dislocations, and then the short-range stress filed is formed around the grain boundary, as displayed in Fig. 9. As a result, the short-range stress field prevents lattice dislocations from entering or passing through grain boundaries, leading to a larger τ^*. Given the above, the incorporation of Cu into the CrFeCoNi HEA causes the increase of yield strength.

The variation in the ultimate tensile strength of $CrFeCoNiCu_x$ alloys can be explained by Arrhenius-type equation, which is often used to characterize the thermally activated glide process [24,25]. Appling such an approach, the strain- dependent flow stress ($\sigma(\varepsilon)$) can be expressed as

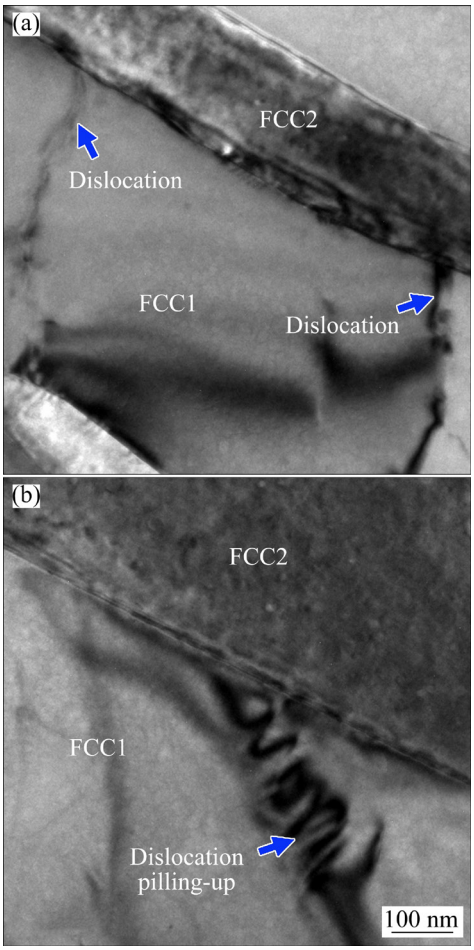

Fig. 9 Deformed microstructure of Cu-containing HEA: (a) Hindrance of FCC1/FCC2 boundary to dislocations sliding; (b) Dislocation piling-up at front of boundary

$$\sigma(\varepsilon)=\sigma_0+\sigma_u(\varepsilon)+\sigma^*(\varepsilon) \quad (3)$$

where σ_0 is the stress contribution arising from the thermal and athermal mechanisms operated at the onset of the yielding, and is considered to be independent of strain (ε). $\sigma_u(\varepsilon)$ means an athermal stress contribution to work-hardening which originates from long-range dislocations. $\sigma^*(\varepsilon)$ represents the effective or thermal stress component owing to thermally assisted overcoming of the deformation-induced short-range glide obstacles. Similar to the yield strength analysis, the intensification of lattice distortion and the increase in the proportion of grain boundaries enhance the short-range barriers to dislocation glide, thus leading to the increase of $\sigma^*(\varepsilon)$. Therefore, the ultimate tensile strength is improved with the increase of Cu additions. However, the decrease of fracture elongation caused by the increase of Cu content is mainly caused by dislocation pile-up at

grain boundaries. It is known that dislocation pile-up at grain boundary not only causes great stress concentration at grain boundary, but also produces certain stress filed in front of grain boundary. It will lead to the initiation of micro-cracks when the stress field exceeds a critical level. Under the condition of Cu additions, the proportion of the grain boundary is greatly increased and the stress field caused by dislocations accumulated at grain boundaries is increased correspondingly during tensile deformation process. The initiation and propagation of micro-cracks become much easier with the assistance of superposition of more stress fields, thus leading to premature failure.

Figure 10 shows the fracture morphologies of the CrFeCoNiCu$_x$ alloys after tensile test. It is evident that there are a large number of dimples on the fracture surfaces of all the samples, presenting the typical characteristics of ductile fracture. But it should be noted that the morphology of dimples changes obviously with the addition of Cu. For the Cu$_0$ alloy, the dimples on the fracture are equiaxial and deep, indicating excellent plastic deformation ability. However, with the increase of Cu additions, the dimples on the facture become elongated and shallow. In general, dimples are formed by the condensation of micro-pores produced during deformation, and the geometry of dimples mainly depends on the stress acting on the micro-pores. Under the action of tensile stress, the micro-pores can grow along the plane. In the present work, incorporation of Cu leads to the formation of FCC2 phase in the Cu-containing alloys, and due to the difference in the resistance of FCC1 and FCC2 phases to micro-pores propagation, the micro-pores will expand easily within the softer phase, while their propagation towards the hard phase is restricted. Therefore, the dimples on the facture surfaces of Cu$_{0.3}$, Cu$_{0.5}$ and Cu$_{0.7}$ alloys present the elongated and shallow characteristics, indicting a decrease in the plastic deformation ability.

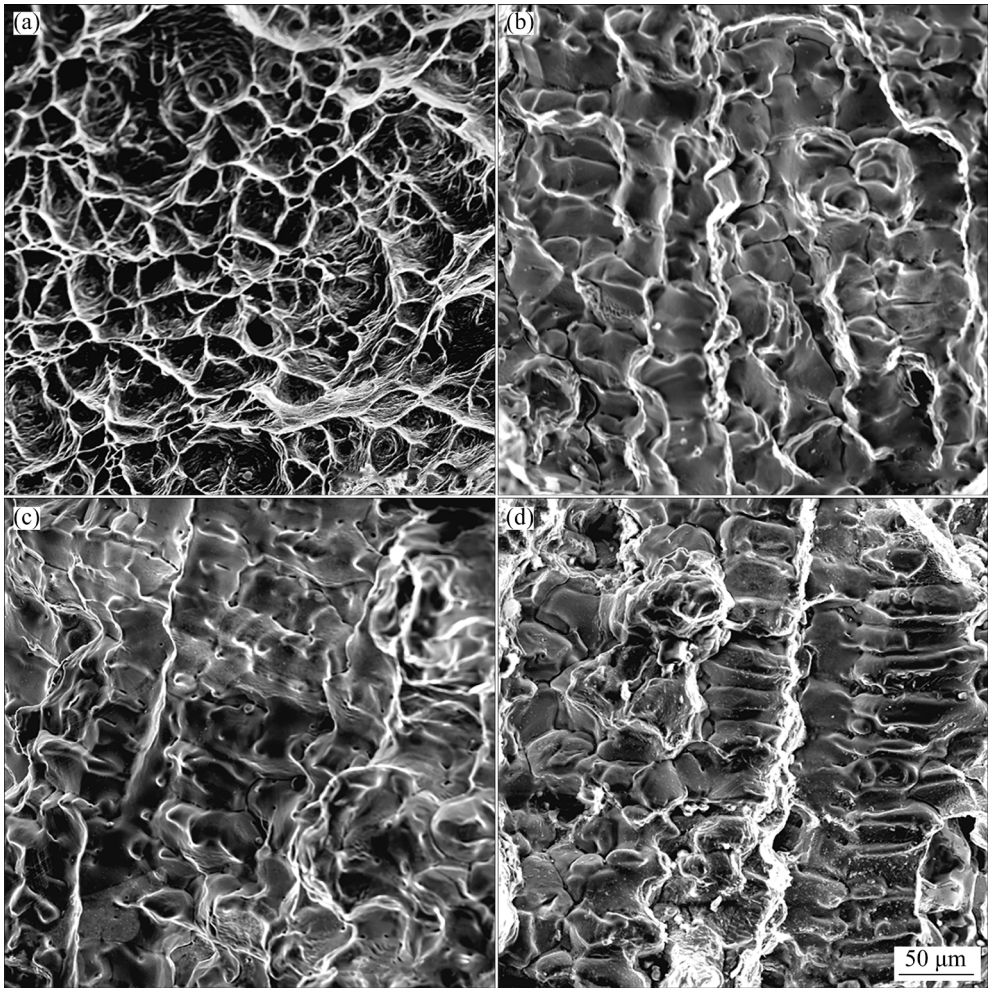

Fig. 10 Fracture morphologies of CrFeCoNiCu$_x$ alloys: (a) Cu$_0$; (b) Cu$_{0.3}$; (c) Cu$_{0.5}$; (d) Cu$_{0.7}$

4 Conclusions

(1) The addition of Cu promotes the phase constituent of the CrFeCoNi HEA from single FCC phase to FCC1 plus FCC2 phase. The lattice constant of FCC1 phase decreases with the increase of Cu content, while the lattice constant of FCC2 phase versus the Cu content presents an opposite trend.

(2) The FCC2 phase is determined to be Cu-rich phase existing in the inter-dendrite region. An increase in the Cu content leads to a larger volume fraction of FCC2 phase, and the Cu_0, $Cu_{0.3}$, $Cu_{0.5}$ and $Cu_{0.7}$ alloys contain 0, 2.6, 3.4, 7.6 vol.% FCC2 phase, respectively.

(3) The yield strength and ultimate tensile strength are enhanced with the increase of Cu content. The improvement of strength is mainly due to the increase of short-range obstacles to dislocation slip. The superposition of stress filed caused by the dislocation piling-ups at grain boundaries leads to a successive drop in the fracture strain of Cu_0, $Cu_{0.3}$, $Cu_{0.5}$ and $Cu_{0.7}$ alloys.

(4) The fracture surfaces of $CrFeCoNiCu_x$ alloys contain a large number of dimples, indicating the typical feature of ductile fracture. However, as the Cu content increases, the regular and deep dimples become elongated and shallow.

Acknowledgments

The authors would like to thank the support of the National Natural Science Foundation of China (Nos. 52001236, 51971099), the Natural Science Foundation of Hubei Province, China (No. 2020CFB113), and the Open Fund of State Key Laboratory of Materials Processing and Die & Mould Technology, China (No. P2022-010).

References

[1] YEH J W, CHEN S K, LIN S J, GAN J Y, CHIN T S, SHUN T T, TSAU C H, CHANG S Y. Nanostructured high-entropy alloys with multiple principal elements: Novel alloy design concepts and outcomes [J]. Advanced Engineering Materials, 2004, 6(5): 299−303.

[2] CANTOR B, CHANG I T H, KNIGHT P, VINCENT A J B. Microstructural development in equiatomic multicomponent alloys [J]. Materials Science and Engineering A, 2004, 375/376/377: 213−218.

[3] ZHANG Lin, SONG Ruo-kang, QU Guo-xin, LU Tong. Effect of nitrogen on microstructure and mechanical properties of $CrMnFeVTi_6$ high entropy alloy [J]. Transactions of Nonferrous Metals Society of China, 2021, 31: 2415−2427.

[4] LI Z M, PRADEEP K G, DENG Y, RAABE D, TASAN C C. Metastable high-entropy dual-phase alloys overcome the strength−ductility trade-off [J]. Nature, 2016, 534(7606): 227−230.

[5] ERDOGAN A, DOLEKER K M. Comparative study on dry sliding wear and oxidation performance of HVOF and laser re-melted $Al_{0.2}CrFeNi(Co,Cu)$ alloys [J]. Transactions of Nonferrous Metals Society of China, 2021, 31: 2428−2441.

[6] ERDOGAN A, SUNBUL S E, ICIN K, DOLEKER K M. Microstructure, wear and oxidation behavior of AlCrFeNiX (X=Cu, Si, Co) high entropy alloys produced by powder metallurgy [J]. Vacuum, 2021, 187: 110143.

[7] SENKOV O N, MIRACLE D B, CHAPUT K J, COUZINIE J P. Development and exploration of refractory high entropy alloys—A review [J]. Journal of Materials Research, 2018, 33(19): 3092−3128.

[8] CAO Yuan-kui, LIU Yong, LIU Bin, ZHANG Wei-dong, WANG Jia-wen, DU Meng. Effects of Al and Mo on high temperature oxidation behavior of refractory high entropy alloys [J]. Transactions of Nonferrous Metals Society of China, 2019, 29: 1476−1483.

[9] CHOU H P, CHANG Y S, CHEN S K, YEH J W. Microstructure, thermophysical and electrical properties in $Al_xCoCrFeNi$ ($0\leq x\leq 2$) high-entropy alloys [J]. Materials Science and Engineering B, 2009, 163(3): 184−189.

[10] WANG W R, WANG W L, WANG S C, TSAI Y C, LAI C H, YEH J W. Effects of Al addition on the microstructure and mechanical property of $Al_xCoCrFeNi$ high-entropy alloys [J]. Intermetallics, 2012, 26: 44−51.

[11] BEYRAMALI KIVY M, ZAEEM ASLE M. Generalized stacking fault energies, ductilities, and twin abilities of CoCrFeNi-based face-centered cubic high entropy alloys [J]. Scripta Materialia, 2017, 139: 83−86.

[12] ZHENG Fu-kai, ZHANG Guan-nan, CHEN Xiu-juan, YANG Xiao, YANG Zeng-chao, LI Yong, LI Jiang-tao. A new strategy of tailoring strength and ductility of CoCrFeNi based high-entropy alloy [J]. Materials Science and Engineering A, 2020, 774: 138940.

[13] GEORGE E P, RAABE D, RITCHIE R O. High-entropy alloys [J]. Nature Reviews Materials, 2019: 4(8): 515−534.

[14] ZHANG L J, YU P F, FAN J T, ZHANG M D, ZHANG C Z, CUI H Z, LI G. Investigating the micro and nanomechanical properties of $CoCrFeNiC_x$ high-entropy alloys containing eutectic carbides [J]. Materials Science and Engineering A, 2020, 796: 140065.

[15] HE J Y, WANG H, HUANG H L, XU X D, CHEN M W, WU Y, LIU X J, NIEH T G, AN K, LU Z P. A precipitation-hardened high-entropy alloy with outstanding tensile properties [J]. Acta Materialia, 2016, 102: 187−196.

[16] PENG Jian, LI Zi-yong, JI Xin-bo, SUN Yan-le, FU Li-ming, SHAN Ai-dang. Decomposition kinetics of carbon-doped FeCoCrNiMn high-entropy alloy at intermediate temperature [J]. Transactions of Nonferrous Metals Society of China, 2020, 30: 1884−1894.

[17] DASARI S, JAGETIA A, CHANG Y J, SONI V, GWALANI

B, GORSSE S, YEH A C, BANERJEE R. Engineering multi-scale B2 precipitation in a heterogeneous FCC based microstructure to enhance the mechanical properties of a $Al_{0.5}Co_{1.5}CrFeNi_{1.5}$ high entropy alloy [J]. Journal of Alloys and Compounds, 2020, 830: 154707.

[18] WANG W L, HU L, LUO S B, MENG L J, GENG D L, WEI B. Liquid phase separation and rapid dendritic growth of high-entropy CoCrCuFeNi alloy [J]. Intermetallics, 2016, 77: 41−45.

[19] YE Y F, WANG Q, LU J, LIU C T, YANG Y. High-entropy alloy: Challenges and prospects [J]. Materials Today, 2016, 19(6): 349−362.

[20] WU P H, LIU N, YANG W, ZHU Z X, LU Y P, WANG X J. Microstructure and solidification behavior of multi-component $CoCrCu_xFeMoNi$ high-entropy alloys [J]. Materials Science and Engineering A, 2015, 642: 142−149.

[21] DABROWA J, CIEŚLAK G, STYGAR M, MROCZKA K, BERENT K, KULIK T, DANIELEWSKI M. Influence of Cu content on high temperature oxidation behavior of $AlCoCrCu_xFeNi$ high entropy alloys (x = 0; 0.5; 1) [J]. Intermetallics, 2017, 84: 52−61.

[22] LI Cheng, XUE Yun-fei, HUA Mu-tian, CAO Tang-qing, MA Li-li, WANG Lu. Microstructure and mechanical properties of $Al_xSi_{0.2}CrFeCoNiCu_{1-x}$ high-entropy alloys [J]. Materials & Design, 2016, 90: 601−609.

[23] WANG Qiang, ZENG Liang-cai, GAO Teng-fei, DU Hui, LIU Xin-wang. On the room-temperature tensile deformation behavior of a cast dual-phase high-entropy alloy $CrFeCoNiAl_{0.7}$ [J]. Journal of Materials Science & Technology, 2021, 87: 29−38.

[24] WANG Qiang, DING Hong-sheng, ZHANG Hai-long, LIU Shi-qiu, CHEN Rui-run, GUO Jing-jie, FU Heng-zhi. Microstructure and compressive properties of directionally solidified Er-bearing TiAl alloy using cold crucible [J]. Materials & Design, 2016, 99: 10−20.

[25] APPEL F, WAGNER R. Microstructure and deformation of two-phase γ-titanium aluminides [J]. Materials Science and Engineering R, 1998, 22: 187−268.

Cu 添加量对铸态 $CrFeCoNiCu_x$ 高熵合金显微组织和力学性能的影响

胡 强[1]，王海玲[2]，钱立华[2]，曾良才[3,4]，王 强[3,4]，刘鑫旺[5]

1. 江西省科学院 应用物理研究所，南昌 330029；
2. 华中科技大学 物理学院，武汉 430074；
3. 武汉科技大学 机械自动化学院 冶金装备及其控制教育部重点实验室，武汉 430081；
4. 武汉科技大学 机械自动化学院 机械传动与制造工程湖北省重点实验室，武汉 430081；
5. 华中科技大学 材料科学与工程学院 材料成形与模具技术国家重点实验室，武汉 430074

摘 要：详细研究 Cu 添加量对铸态 CrFeCoNi 高熵合金显微组织演变和室温拉伸性能的影响。研究结果表明，添加 Cu 元素使高熵合金相结构由 FCC 单相转变为 FCC1+FCC2 双相。FCC2 相是存在于枝晶间的富 Cu 相，且其体积分数随 Cu 含量的增加而提高。富 Cu 相的形成主要归因于 Cu 与其他金属元素的混合焓较大，从而导致凝固之前的液相分离。由于位错滑移的短程障碍增强，高熵合金的屈服强度和极限抗拉强度与 Cu 含量呈正相关关系。然而，由于位错在晶界堆积而产生的应力场叠加更为显著，因此，含 Cu 高熵合金的断裂应变较小。

关键词：高熵合金；富 Cu 相；显微组织；抗拉强度；断裂应变

(Edited by Wei-ping CHEN)